JOURNAL OF SOLID STATE CHEMISTRY 53, 303–312 (1984)

Changes in Crystallite Size and Microstrains of Hematite Derived from the Thermal Decomposition of Synthetic Akaganeite

J. MORALES, J. L. TIRADO, AND M. MACIAS*

Departamento de Química Inorgánica, Facultad de Ciencias, Universidad de Córdoba, Spain

Received October 15, 1983; in revised form February 8, 1984

The thermal decomposition of akaganeite, β-FeOOH, in air is studied. The structural properties of the dehydroxylation product, identified as hematite, are determined at different temperatures. From the results on crystallite size and microstrains, a change of crystallite shape has been shown to occur in the range of temperatures of 300 to 485°C. A marked increase in crystallite size and a diminution in microstrains is observed at 525°C. This change is related to the occurrence of an exothermic peak in the DTA and DSC curves of akaganeite at about 512°C. The peak is thus ascribed to a recrystallization process of hematite. Electron micrographs support the most relevant observations of changes in particle size and shape.

Introduction

The DSC and DTA curves of synthetic akaganeite, β-FeOOH, show a multiple endothermic peak due to the dehydroxylation process, as well as a sharp exotherm near 450°C (*1*). This exothermic peak has been interpreted in various ways, depending on the nature of the sample and the conditions of recording of the DTA curves. González-Calbet *et al.* (*2*) studied the thermal decomposition of akaganeite under vacuum. These authors identify the dehydroxylation product as γ-Fe_2O_3 and ascribe the exotherm observed in air to the transformation of maghemite into hematite, an explanation first suggested by Mackay (*3*). On the other hand, Naono *et al.* (*4*) show that the X-ray diffraction patterns of the dehydroxylation product in a vacuum contain no reflections, due to the presence of ultrafine crystals of decomposed β-FeOOH. This phase transforms into α-Fe_2O_3 with increasing temperature.

The thermal decomposition of akaganeite in nitrogen and oxygen atmospheres was recently studied by Paterson *et al.* (*5*). These authors show that a different but poorly crystallized phase occurs in each atmosphere after dehydroxylation. These phases change particle shape and increase crystallinity at higher temperatures, probably producing the exotherm, although the peak is also associated with the loss of chlorine in a N_2 atmosphere. From this work, some doubts about the nature of the exothermic effect arise. The aim of this paper is to examine the products obtained at different stages of the DTA curve of synthetic akaganeite in order to provide a consistent explanation of the exothermic peak.

* Actual address: Dpto. Química Inorgánica, Facultad de Química, Sevilla, Spain.

0022-4596/84 $3.00

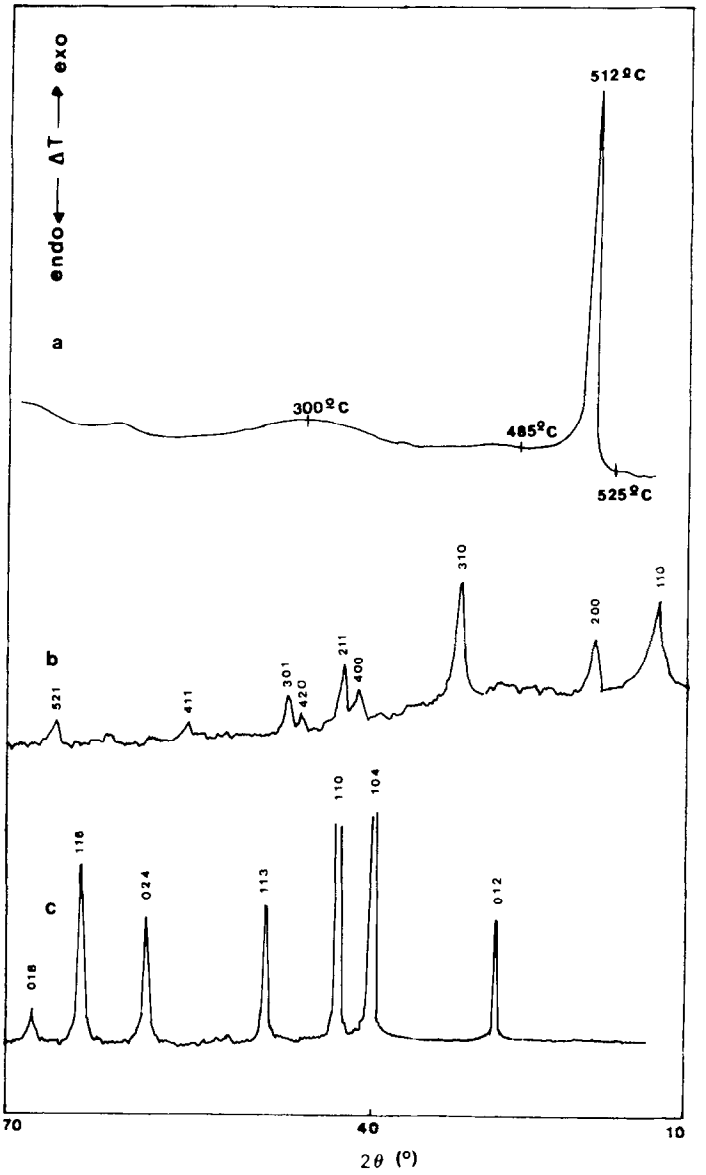

FIG. 1. (a) DTA curve of synthetic akaganeite in air, showing the temperature of the exothermic peak (512°C) and those used in the preparation of decomposed samples. (b) X-Ray diffraction pattern of synthetic akaganeite. (c) X-Ray diffraction pattern of the sample obtained at 300°C, showing hematite reflections exclusively.

Experimental

The synthetic sample of β-FeOOH was prepared by the hydrolysis at 70°C of an aqueous solution of iron(III) chloride (2% in weight). The precipitate was aged for 15 days, separated in a centrifuge, and washed until peptization occurred. The X-ray diffraction pattern of the sample (see Fig. 1) shows exclusively the reflections of akaganeite.

A differential thermal analysis was performed on a Stanton Redcroft 673-4 thermoanalyzer in static air atmosphere. Decomposed samples at 300, 485, and 525°C were obtained by interrupting the DTA experiment. These samples were used in the remaining determinations.

Differential scanning calorimetry was carried out on a Mettler TA 300 apparatus provided with a TA processor unit that was used to obtain the integrated ΔH and peak temperature.

Electron micrographs were performed on a Phillips EM 300. The samples were dispersed in acetone by ultrasound and settled on copper grids for examination.

X-Ray diffraction patterns were recorded on a Phillips PW 1130 diffractometer, using CoKα radiation and Fe filter. X-Ray diffraction line profiles were recorded by continuous scan at 0.125° min^{-1} and the intensities were read each 0.025° 2θ. A line profile analysis was carried out in the (104), (110), (024), and (116) reflections of hematite. These lines were chosen for their high peak to background ratio and the absence of overlapping peaks. A highly crystalline hematite sample ("Merck" Fe_2O_3 annealed at 800°C during 4 hr) provided the instrumental profiles. Centroid position and background level were corrected by means of a computer program based in that of Edwards and Toman (*6*). The determination of crystallite size and microstrains was developed by four different methods in order to avoid a biased interpretation of the results.

In first instance, the slope of the integrated intensity versus reciprocal range curve (k_1) was used to obtain an estimate of the apparent crystallite size (ε_{k1}) which was computed after the subtraction of k_{1g} from k_{1h}, without correcting truncation errors, as it is specified by Langford (*7*). The linear extrapolation of this curve provided values for the total intensity of the line (S_∞). From these data, the integral breadths were calculated and the Jones correction of instrumental broadening was performed. A new estimate of crystallite size (D) was computed from the corrected integral breadths (β) by the Scherrer equation.

From the slope (k) and intercept (W_0) of the variance-range curves of the g and h profiles corrected for truncation (*7*), the slope and intercept of the f profiles were obtained. Slopes were simply subtracted while the intercepts were corrected for the nonadditivity error according to

$$k_f = k_h - k_g$$
$$W_{0_f} = W_{0_h} - W_{0_g} - \pi^2 k_f k_g/2. \quad (1)$$

The values of k_f and W_{0_f} were used in the computation of apparent crystallite size (ε_k) and the variance of the lattice strain distribution ($\langle e^2 \rangle$) by means of the equation of Langford and Wilson (*8*), in which:

$$k_f = \lambda/(\pi^2 \varepsilon_k \cos\theta)$$
$$W_{0_f} = 4 \tan^2\theta \langle e^2 \rangle - \lambda^2/(4\pi^2 \varepsilon_k^2 \cos^2\theta). \quad (2)$$

Where λ is the radiation wavelength and θ the angle of the line centroid.

Finally, the cosine Fourier coefficients of the f profiles obtained by the Stokes method (*9*) were used to calculate the average crystallite size perpendicular to the reflecting planes (ε_F). These values and an alternative evaluation of microstrains ($\langle e \rangle_F$) were computed by using the Fourier-space method developed by Smith (*10*), in which the Fourier coefficients (A_n) are adjusted by curve fitting to Bertaut's equation (*11*), stated as

$$A_n = (1 - an/\varepsilon_F)\cos(2\pi l \langle e \rangle n). \quad (3)$$

Where

$$a = \lambda/4(\sin\theta_m - \sin\theta_0)$$
$$l = 2a \sin\theta_0/\lambda. \quad (4)$$

Where θ_0 is the angle of the centroid and $\theta_0 - \theta_m$ is the period of expansion of the Fourier series.

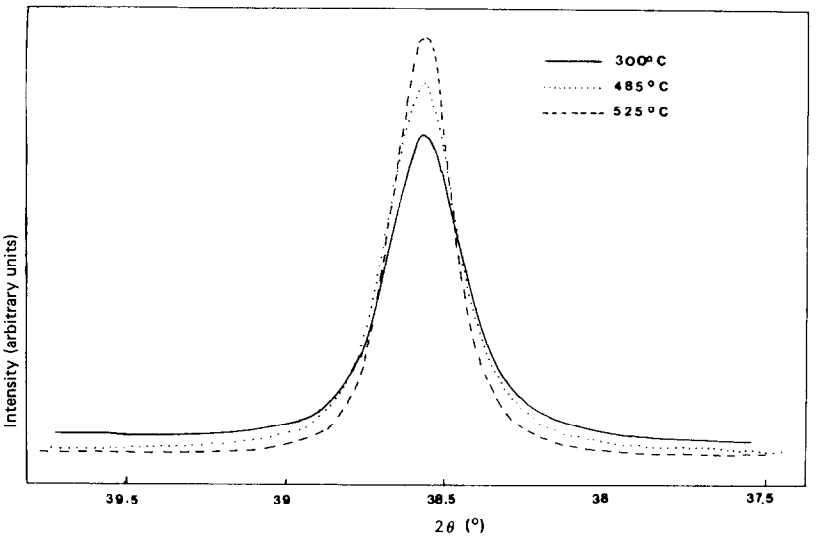

FIG. 2. X-Ray diffraction line profiles of the (104) reflections of hematite obtained at 300, 485, and 525°C. A decrease of the broadening on increasing temperature is observed.

The relatively poor accuracy of these single-line methods is, however, unavoidable, because of the anisotropy of crystallite size and microstrains and the absence of multiple order reflections in more than one crystallographic direction.

Results and Discussion

Figure 1a shows a typical DTA curve of synthetic akaganeite recorded in air atmosphere. The sharp exothermic peak occurs at approximately 510°C. The DSC curve is identical in shape, yielding values of ΔH of 153 J g^{-1} for the integrated peak. Three samples of decomposed akaganeite were prepared by interrupting the DTA experiment at the temperatures shown in Fig. 1a. The lowest temperature (300°C) was selected in order to characterize the initial product of dehydroxylation, while the other temperatures provide samples whose differences are able to explain the exothermic effect. The X-ray diffraction patterns of these three samples show the same reflections which allow the identification of the product of dehydroxylation as hematite (see, for example, Fig. 1b). The lines of hematite are especially broadened for the samples obtained at 300 and 485°C, while a marked increase in crystallinity is observed after the exothermic peak is developed (525°C) (Fig. 2). Nevertheless, no other phase seems to be present in the samples. These results agree in part with those found by Paterson *et al.* (*5*) in nitrogen atmosphere, except for the absence of any phase structurally related to β-FeOOH. On the other hand, the differences with the products obtained in a vacuum (*2, 4*) are marked. Thus, the exotherm observed in air cannot be ascribed to a transformation of γ-Fe_2O_3 into hematite.

Since the most important difference between samples obtained at 485 and 525°C involves their crystallinity, the X-ray diffraction line profile analysis may provide a quantitative evaluation of the changes developed through the exothermic peak in terms of crystallite size and microstrains. Table I contains the results of the various methods of line profile analysis applied to

TABLE I

CRYSTALLITE SIZE AND MICROSTRAINS DETERMINATION: RESULTS OF INTEGRAL BREADTH, FOURIER, AND VARIANCE METHODS

	h	k	l	σ_2/FWHM	P/Bk	$b \times 10^3$	$\Delta S/S_\infty$	S_∞	$k_1 \times 10^4$	$\Delta k/k$	$W_0 \times 10^7$	$k \times 10^4$
	1	0	4	4.13	28.2	4.27	3.34	9.8	4.69	3.65	1.72	4.91
	1	1	0	3.88	17.0	4.53	4.11	10.4	5.60	4.59	−4.45	5.92
	0	2	4	3.38	7.1	5.15	3.42	11.8	5.09	3.69	9.49	5.26
	1	1	6	3.19	8.8	5.33	3.60	12.2	5.36	3.89	11.65	5.76

g Profiles: Hematite annealed at 800°C for 4 hr

Sample	h	k	l	σ_2/FWHM	P/Bk	$B \times 10^3$	$\beta \times 10^3$	D	$\Delta S/S_\infty$	S_∞	$k_{1f} \times 10^4$	ε_{k1}	$\Delta k/k_1$	$W_{0_f} \times 10^7$	$k_f \times 10^4$	ε_k	$\sqrt{\langle e^2 \rangle} \times 10^3$	ε_F	$\langle e \rangle_F \times 10^3$
525°C	1	0	4	4.06	18.6	5.11	1.02	1860	4.66	11.7	2.61	736	5.09	−3.65	2.68	718	—	1089	0.48
	1	1	0	4.00	11.7	5.59	1.29	1485	7.23	12.8	5.40	358	8.12	−20.00	5.48	354	—	796	0.47
	0	2	4	3.98	6.0	7.07	2.33	879	6.44	16.2	7.51	276	7.08	−30.39	7.65	272	—	472	0.70
	1	1	6	4.00	7.2	6.81	1.97	1070	5.28	15.6	4.73	450	6.21	−16.63	4.85	440	—	568	0.61
485°C	1	0	4	4.95	14.0	6.54	2.81	675	4.31	15.0	5.02	384	4.83	−4.84	5.50	350	0.73	446	0.95
	1	1	0	4.98	9.2	6.60	2.51	763	4.65	15.1	5.09	380	5.57	−7.19	6.00	322	0.55	398	1.10
	0	2	4	4.43	3.8	9.29	5.11	401	5.69	21.3	10.37	200	6.36	−24.48	10.86	192	0.59	320	1.00
	1	1	6	3.94	4.9	9.91	5.65	373	5.67	22.7	10.00	214	6.21	−23.59	10.48	204	0.47	306	1.03
300°C	1	0	4	5.05	11.1	6.71	3.02	629	4.36	15.4	5.72	336	4.85	−8.47	6.17	312	0.43	391	1.20
	1	1	0	4.90	7.9	6.11	1.89	1013	5.28	14.0	6.07	320	6.08	−16.69	6.54	296	—	439	0.98
	0	2	4	4.50	3.3	8.98	4.76	431	4.72	20.6	8.75	236	5.23	−17.73	9.23	224	0.53	345	0.99
	1	1	6	4.50	4.4	8.65	4.07	518	3.75	19.8	5.16	414	3.91	−5.10	5.11	418	0.29	452	0.73

σ_2/FWHM	Maximum range of scan (in FWHM units)	P/Bk	Peak to background ratio
B,b, and β	Integral breadths of h, g, and f profiles (from S_∞)	D	Mean crystallite size (Scherrer) (Å)
$\Delta S/S_\infty$	Percentage of integrated intensity lost by truncation	$\varepsilon_{k,k1,F}$	Apparent crystallite sizes from k_f, k_{1f}, and Fourier analysis (Å)
S_∞	Total integrated intensity (normalized)	k	Slope of the variance–σ curves (rad) } truncation
$\Delta k/k$	Correction for truncation (percentage)	$W0$	Intercept of the variance–σ curves (rad^2) } corrected
$\sqrt{\langle e^2 \rangle}$, $\langle e \rangle$	Microstrains from W_{0_f} and Fourier analysis	k_1	Slope of the intensity–σ^{-1} curves (rad)

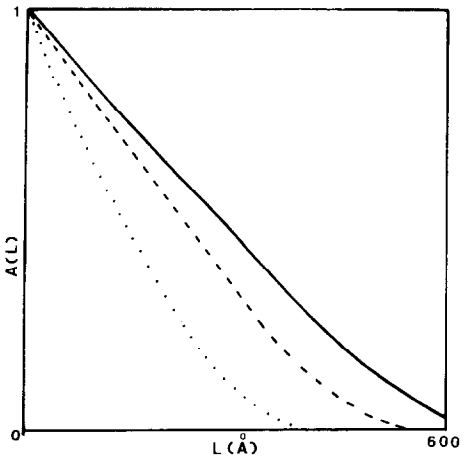

FIG. 3. Cosine Fourier coefficients $A(L)$ of the (116) reflection of hematite as a function of L (—, 525°C; ---, 300°C; · · ·, 485°C).

the (104), (110), (024), and (116) reflections of hematite. In these results, one should note the important divergences observed between the values of crystallite size obtained from the variance, Fourier, and Scherrer methods. Similar discrepancies have been pointed out by Guilliatt and Brett (*12*), and Louër *et al.* (*13*), and seem to be inherent to the application of these methods. No correction for truncation was carried out in the Fourier coefficients. However, the contribution of truncation errors to the so-called "hook" effect, first recognized by Bertaut (*14, 15*), seems to be absent, as is shown in Fig. 3. On the contrary, an important relation is found between the values of ε_k and ε_{k1} which is consistent with the assumption of Lorentzian tails of the profiles. Some of the integrated intensity, I_{max}, versus reciprocal maximum range curves of the h profiles are plotted in Fig. 4. A significant linearity is observed, that yields for the values of $k1$ an accuracy similar to that of the variance-range slopes, once the background is correctly eliminated. On the other hand, it is interesting to note that truncation errors ($\Delta k/k$) are generally low and close to the percentages of integrated intensity lost by truncation ($\Delta S/S_\infty$). According to Langford (*7*), truncation can remove about 5% of the integrated intensity of a typical profile, and the values of $\Delta k/k$ should not exceed 15%. These requirements are fulfilled by the results included in Table I.

Concerning the values of maximum range of scan (σ_2/FWHM), it must be noted that their relationship with $\Delta S/S_\infty$ also depends on crystallite shape (*7*). This fact might result in the lack of a clear correlation between both parameters (see Table I).

The results of microstrain determination from the intercept of the variance-range plots and the Fourier analysis differ in magnitude, although their changes with temperature are similar. This divergence may arise from the different approaches inherent to each method, which lead to different concepts of microstrains.

When the values of crystallite size obtained for each reflection of a sample are compared, a notorious anisotropy can be observed from Table I. This fact is explained by the assumption of an irregular crystallite shape, as has been studied by Duvigneaud and Derie (*16*) for the case of

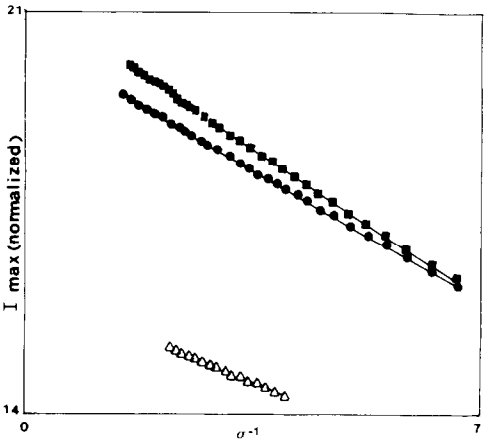

FIG. 4. Variation of integrated intensity with σ^{-1} in the tails of the (024) line profiles of hematite (■, 485°C; ●, 300°C; △, 525°C).

hematite derived from goethite. However, a cylindrical or acicular shape cannot be clearly identified (see, for example, column ε_F in Table I). Nevertheless, the highest ratio of crystallite size between the (110) and (104) reflections occurs for the sample heated at 300°C. This behavior may be considered representative of a tubular or acicular shape (*16, 17*).

Moreover, several significant changes in crystallite size and shape and microstrains are observed in hematite after the dehydroxylation of β-FeOOH. From 300 to 485°C small variations occur in crystallite size and microstrains, although a differential broadening of the lines is encountered. In this way, crystallite size obtained for the (116) lines decreases markedly, whatever the method used in calculation. A similar diminution in this parameter is observed for the (024) line, although the changes are not so marked. By contrast, no significant decrease in crystallite size is obtained for the (104) reflection. As has been pointed out above, these results could be explained in terms of either a change of crystallite shape (*16*), or by the presence of stacking faults in the packing of oxygen layers at low temperature (*18*). However, the former explanation seems to be supported by the electron micrographs, as will be discussed below.

Preferential line broadening in goethite-derived hematite was recently studied by Yamaguchi and Takahashi (*19*), but the results reported by these authors disagree with those contained in Table I. Taking into account the different oxyhydroxide that leads to hematite and the absence of an exothermic peak after the dehydroxylation of goethite, considerations of line broadening are not comparable in both cases.

On the other hand, once the exothermic peak is developed, hematite shows an important increase in crystallite size, whereas microstrains remain within the experimental errors in the variance method and decrease considerably (more than a 50%) in the Fourier method. If we take into account the small interval of temperatures which separates the samples obtained at 485 and 525°C, the origin of the exotherm can be ascribed to the release of energy stored as internal strains, which is accompanied by a sintering process (Table I). If the broadening could be ascribed exclusively to microstrains, a calculation of the released energy could be performed (*20*), but a contribution from the crystallite size is in evidence. A similar cause has been assigned to other exothermic effects in which the contribution of crystallite size was large enough to be considered, as in the DSC curves of ground dolomite (*21*).

Finally, Fig. 5 shows the electron micrographs of the original akaganeite and the three decomposed samples. Undecomposed akaganeite shows a characteristic spindle shape (Fig. 5a). Similarly, the hematite particles obtained at 300°C have an elongated shape (Fig. 5b) that could explain the high value of crystallite size for the (110) reflection of this sample, that was discussed above, if particle and crystallite are considered to be identical in shape. When hematite is obtained at 485°C, some significant changes take place: the particle size decreases slightly and the observed shape is more rounded at this temperature (Fig. 5c). These results agree partially with the determinations of crystallite size. However, the most important changes in particle size and shape are observed when the samples obtained at 485 and 525°C are compared (Figs. 5c and d). The particle size is especially high at 525°C and thus, provides additional support to the interpretation of the exothermal peak in terms of a sintering process, aside from the decrease in microstrains, as shown in Table I. On the other hand, the assumption of an elongated shape of crystallites, which is not supported by X-ray profile analysis, seems to be inconsistent with the particles observed in Fig. 5d.

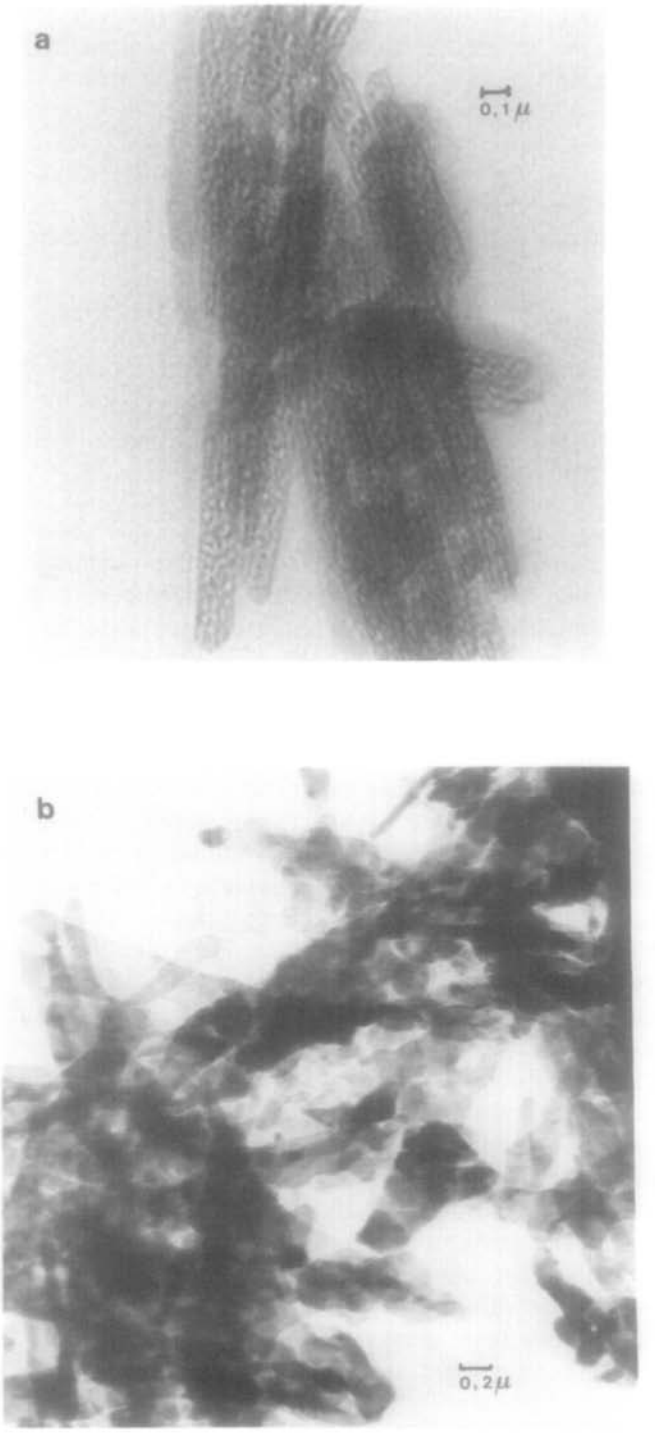

FIG. 5. Electron micrographs of synthetic akaganeite (a), and hematite obtained at 300 (b), 485 (c), and 525°C (d).

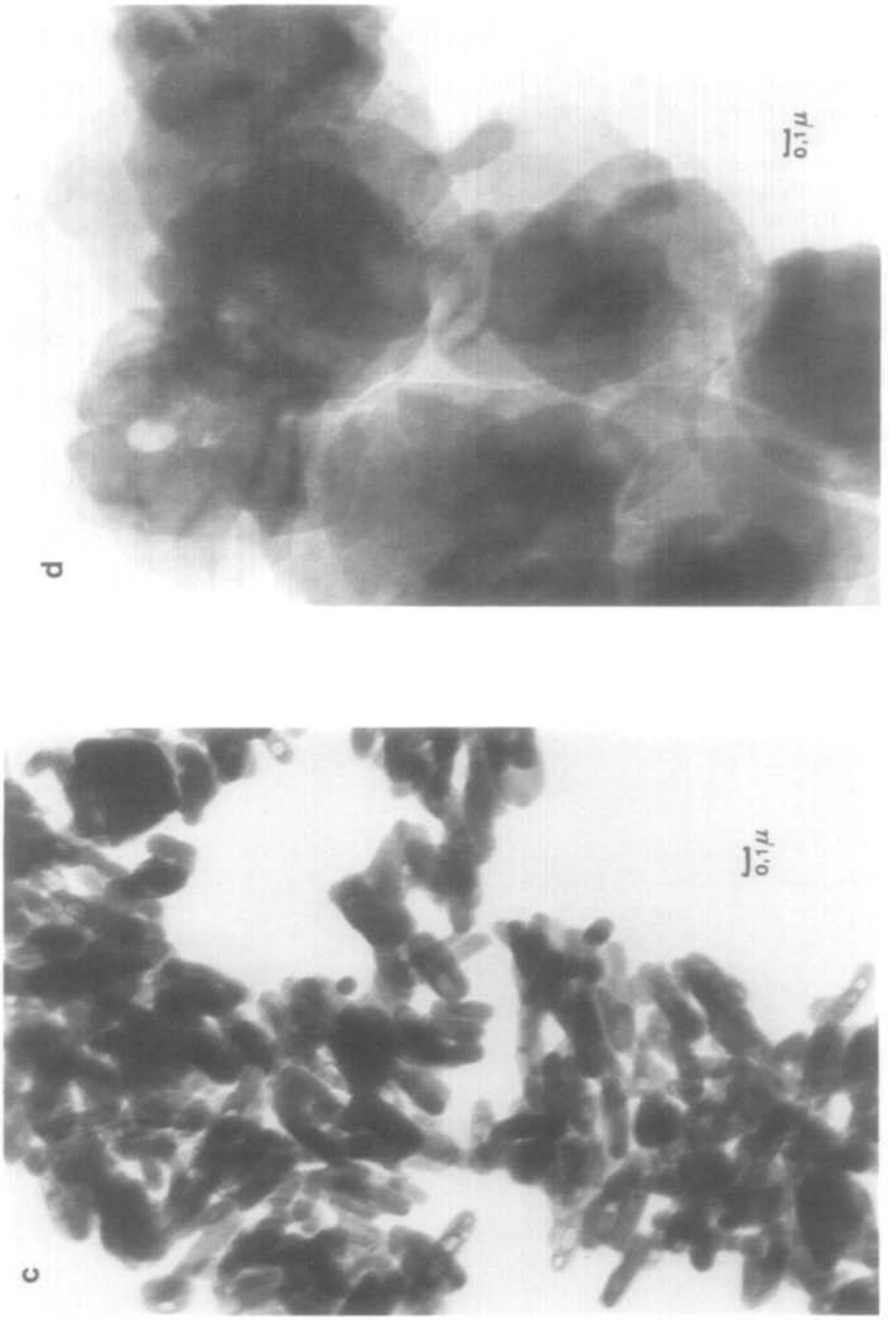

FIG. 5—*Continued.*

References

1. R. C. MACKENZIE AND G. BEGGREN, *in* "Differential Thermal Analysis" (R. C. Mackenzie, Ed.), Vol. 1, Chap. 9, Academic Press, New York (1970).
2. J. M. GONZALEZ CALBET, M. A. ALARIO FRANCO, AND M. GAYOSO ANDRADE, *J. Inorg. Nucl. Chem.* **43,** 257 (1981).
3. A. L. MACKAY, *Mineral. Mag.* **32,** 545 (1960).
4. H. NAONO, R. FUJIWARA, H. SUGIOKA, K. SUMIYA, AND H. YANAZAWA, *J. Colloid Interface Sci.* **87,** 317 (1982).
5. E. PATERSON, R. SWAFFIELD, AND D. R. CLARK, *Thermochim. Acta* **54,** 201 (1982).
6. H. J. EDWARDS AND K. TOMAN, *J. Appl. Crystallogr.* **4,** 332 (1971).
7. J. I. LANGFORD, *J. Appl. Crystallogr.* **15,** 315 (1982).
8. J. I. LANGFORD AND A. J. C. WILSON, *in* "Crystallography and Crystal Perfection" (G. N. Ramachandran, Ed.), pp. 207–222, Academic Press, New York (1963).
9. A. R. STOKES, *Proc. Phys. Soc. London* **61,** 382 (1948).
10. R. S. SMITH, *IBM J. Res. Dev.* **4,** 205 (1960).
11. E. F. BERTAUT, *C.R.* **288,** 492 (1949).
12. I. F. GUILLIATT AND N. H. BRETT, *Philos. Mag.* **21,** 671 (1970).
13. D. LOUËR, J. P. AUFFREDIC, J. I. LANGFORD, D. CIOSMAK, AND J. C. NIEPCE, *J. Appl. Crystallogr.* **16,** 183 (1983).
14. E. F. BERTAUT, *Acta Crystallogr.* **3,** 14 (1950).
15. E. F. BERTAUT, *Acta Crystallogr.* **5,** 117 (1952).
16. P. H. DUVIGNEAUD AND R. DERIE, *J. Solid State Chem.* **34,** 323 (1980).
17. H. NAONO AND R. FUJIWARA, *J. Colloid Interface Sci.* **73,** 406 (1980).
18. J. LIMA DE FARIA, *Z. Kristallogr. Kristallgeom.* **119,** 176 (1973).
19. T. YAMAGUCHI AND T. TAKAHASHI, *J. Amer. Ceram. Soc.* **65,** C-83 (1982).
20. K. A. GROSS, *Philos. Mag.* **12,** 801 (1965).
21. J. MORALES AND J. L. TIRADO, *Mater. Chem. Phys.*, in press.